

INVESTIGATION OF THE INFLUENCE OF INDIRECT SQUEEZE CASTING PROCESS PARAMETERS ON THE SOLIDIFICATION MICROSTRUCTURE AND PROPERTIES OF A356.2 ALUMINUM ALLOY

Xiaolong Jiang, Shuming Xing , Hongji Sun, Guangyuan Yan and Qian Hu

School of Mechanical, Electronic and Control Engineering, Beijing Jiaotong University, Beijing 100044, China

Copyright © 2023 American Foundry Society
<https://doi.org/10.1007/s40962-023-01178-4>

Abstract

Effects of indirect squeeze casting process parameters on the microstructure and mechanical properties of an A356.2 alloy engine hanger were studied. A 4-factor, 4-level orthogonal test was used to study the effects of applied pressure, punch velocity, pouring temperature and mold preheating temperature. The pressure, punch speed, pouring temperature and mold preheating temperature of the optimum process parameters were determined by range analysis (RA) as 100 MPa, 60 mm/s, 700 °C and 200 °C, respectively. The analysis of variance (ANOVA) showed that the only significant factor affecting the microstructure and mechanical properties was pouring temperature, while the other three factors were not significant. The specimens demonstrated mechanical characteristics akin to forged hangers, boasting a tensile strength of 297 MPa, 10.2% post-fracture elongation, and 105 HBW hardness. After T6 heat treatment, except the eutectic silicon morphology

changed significantly, the microstructure basically maintained its as-cast characteristics. The samples' microstructure were categorized into three regions: coarse grain α -Al (A), eutectic structure (B), and fine grain structure (C). It was found that elevated pouring temperature could keep the pressure transmission channel open, which was helpful to improve the feeding ability and form a refined grain structure in zone C. However, with the excessive increase in casting temperature, α -Al grains in region A would be coarse, which would lead to the decline of mechanical properties. Therefore, 700 °C was determined as the best pouring temperature.

Keywords: squeeze casting, orthogonal test, process parameters, A356.2 alloy, microstructure, mechanical properties

Introduction

Squeeze casting, also known as liquid die forging, is a highly efficient and precise forming technology that combines casting and intensification pressure processing characteristics.¹ It finds extensive applications in the automotive, aerospace, and defense industries, producing parts with high-quality and high-precision characteristics.^{2–5} Squeeze casting can be categorized into direct and indirect methods.⁶ There has been extensive research on how direct squeeze casting process parameters affect the microstructure and mechanical properties of castings, aiming to achieve fine microstructures and enhanced mechanical properties.

For instance, Li et al.⁷ compared gravity and squeeze casting Al–xSi alloys, revealing that squeeze casting significantly refines the microstructure, leading to increased mechanical properties. Similarly, Karthik et al.⁸ investigated the effect of process parameters on the density and hardness of AA2219 alloy in the squeeze casting process, identifying applied pressure as the most influential factor. Senthil et al.⁹ studied the effect of indirect squeeze casting process parameters on the mechanical properties of AC2A aluminum alloy castings, where applied pressure, mold preheating temperature, and dwell time were found to be significant influencing factors. These studies have demonstrated the crucial role of pressure in the direct squeeze casting process, as it promotes rapid solidification and grain refinement, ultimately enhancing mechanical properties.

In the context of indirect squeeze casting, Chang et al.¹⁰ highlighted the importance of gating speed during cavity

Table 1. A356.2 Aluminum Alloy Material Composition

Elements	Al	Si	Fe	Cu	Mg	Ti
Wt%	Bal.	7.1	0.11	0.02	0.45	0.11

Table 2. Material Composition of Forging Hanger

Elements	Al	Mg	Si	Cu	Cr	Ti	Fe	Zn	Mn
Wt%	Bal.	0.9	0.62	0.20	0.08	0.02	0.27	0.02	0.07

filling, affecting the microstructure and properties of the castings. Other studies by Bin et al.¹¹ and Zhao et al.¹² further explored the impact of pressure on the microstructure and mechanical properties of Al-Si alloys, revealing varying effects with increasing pressure. However, most studies have focused on analyzing the influence of individual factors without comprehensive consideration of their synergistic effects.^{13–17} In order to study the influence of multiple process parameters, a lot of experiments are often needed. Deng et al.¹⁸ proposed a data-driven design method of squeeze casting process parameters based on big data. This method can reduce a lot of test costs. In addition, orthogonal experiments are often used to reduce the number of experiments.

In this work, the effects of applied pressure, punch velocity, pouring temperature and mold preheating temperature on the structure and properties of aluminum alloy engine hanger were studied by orthogonal test. The purpose of this work was to provide a new theoretical basis for the optimization of technological parameters of indirect squeeze casting.

Materials and Methods

Test Material

The raw material used in the squeeze casting process of this study was A356.2 aluminum alloy. In each part of the test, the composition of A356.2 aluminum alloy used was shown in Table 1. The material composition of the 6061 aluminum alloy forged hanger used to compare the performance of the hanger with squeeze casting was shown in Table 2.

Alloy Melting and Hanger Preparation

Before feeding, the 500 kilogram crucible electric resistance furnace should be baked. When the temperature rose by 100 °C, the temperature should be kept for 1 h. When the temperature rises to 800 °C, the temperature should be kept for 1 h, and then the temperature should be lowered to 600 °C. Then, 375 kg A356.2 aluminum ingots were prepared to be fed, and the temperature will continue to be raised until all aluminum ingots were completely melted. After melting,

degassing was carried out with graphite rotor and nitrogen gas, the temperature of aluminum liquid was controlled at 720 ± 10 °C, the speed was 300–400 r/min, the air pressure was 0.4–0.5 MPa, and the degassing time was 10–30 min.

The horizontal-die-clamping vertical-shot squeeze casting machine (HVSC) is a machine with a horizontal clamping unit to a vertical opening die and the shot tube is in the vertical position. It is consistent with the filling method of Vertical-die-clamping Vertical-shot Squeeze Casting machine (VSC) squeeze casting machine. The HVSC-400PL squeeze casting machine was used to prepare the hanger. The maximum clamping force of the equipment was 4550 kN, the maximum injection force was 639 kN, and the injection speed was 20–350 mm/s. The photograph of the squeeze casting machine and the schematic diagram of hanger filling were shown in Figure 1. Utilizing the shot piston, the molten metal is directed upward from the lower inlet port to fill the mold cavity. Once filled, pressure is maintained until the casting solidifies, after which it is extracted. The gas was exhausted through the gap of the parting surface of the mold. The mold was naturally cooled in the air.

Heat Treatment Process

Heat treatment was needed after welding the motor hanger and the frame. The heat treatment process of 6061 aluminum alloy frame was used for the heat treatment of A356.2 aluminum alloy motor hanger. The heat treatment parameters were solid solution temperature 530 ± 5 °C, solid solution time 30 min with furnace temperature rise, holding time 40 min and water quenching; aging temperature 205 °C, aging time 1 h with furnace temperature rise, holding time 1.5 h and air cooling to room temperature.

Mechanical Properties Test Methods

The Brinell hardness of hanger was tested by HBRVS-187.5 hardness tester. Test each batch of control specimens were tested under the same conditions 5 hardness points, after removing the maximum and minimum of value, the arithmetic mean of the remaining 3 points as the final specimen hardness.

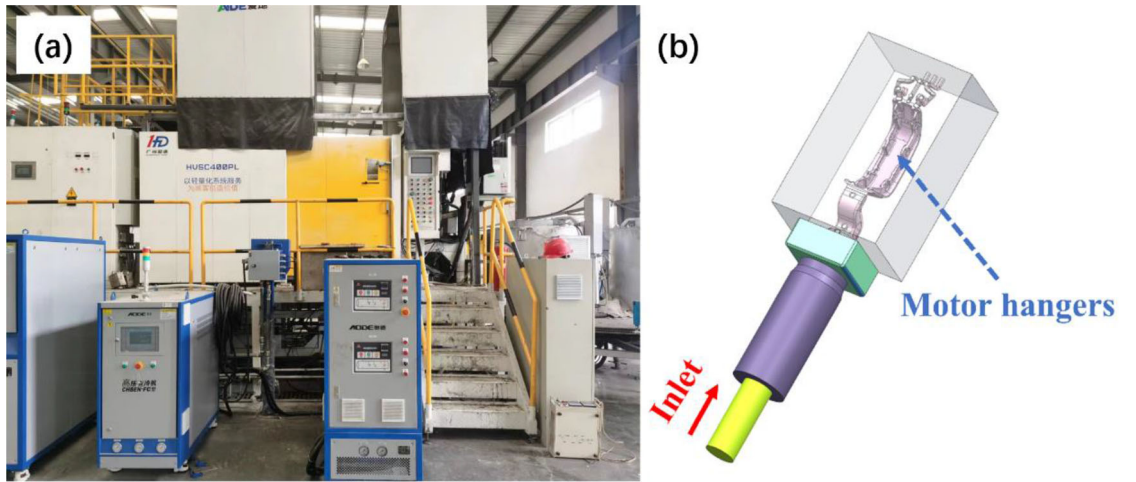


Figure 1. The photograph of the squeeze casting machine and the schematic diagram of hanger filling. (a) The photograph of the squeeze casting machine; (b) the schematic diagram of hanger filling.

The tensile test equipment used WLN10020 microcomputer-controlled pulling and twisting static test machine, the tensile rate was 2 mm/min, and the sampling position was shown in Figure 2.

Metallographic Analysis Methods

The metallographic samples were taken from the clamping part of the tensile specimens, and after rough and fine grinding using 240#, 320#, 600#, 1000#, 2000#, 3000#, 5000# and 7000# sandpaper, polished with the aid of diamond polish with a grain size of 1 μm, and etched for 30 s using Keller's reagent, the metallographic tissue was observed using an Olympus GX53 inverted optical microscope for metallographic observation.

The secondary dendrite arm spacing (SDAS) of the metallographic specimen was measured and counted using the metallographic photo analysis software Image-Pro Plus. The secondary dendrite arm spacing (SDAS) was calculated using Eqn. 1.

$$SDAS = \frac{1}{m} \sum_{j=1}^m \left[\frac{1}{n} \sum_{i=1}^n \frac{L_i}{N-1} \right]_j \quad \text{Eqn. 1}$$

where L_i was the length of the i th secondary dendrite arm, μm; N was the number of secondary dendrite arms; n was the number of statistics; and m was the number of fields of view.

Orthogonal Test

Factors and Levels

In this study, a four-factor, four-level orthogonal test method was used to investigate the influence of process

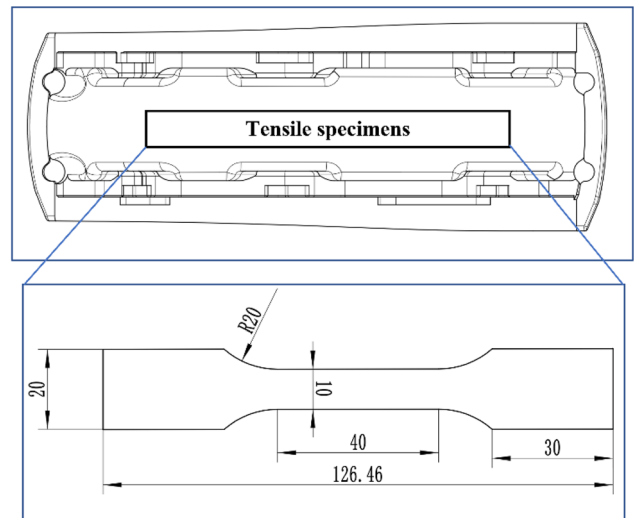


Figure 2. Sampling position and size.

parameters on the as-cast properties of squeeze casting hangers. The influencing factors were applied pressure (A), punch velocity (B), pouring temperature (C), and mold preheating temperature (D). The four levels of applied pressure were selected as 50 MPa, 80 MPa, 100 MPa and 125 MPa; the four levels of punch velocity were 30 mm/s, 40 mm/s, 50 mm/s, and 60 mm/s; the four levels of pouring temperature were 660 °C, 680 °C, 700 °C and 720 °C; and the four levels of mold preheating temperature were 150 °C, 200 °C, 250 °C and 300 °C, as shown in Table 3.

Orthogonal Test Protocol Design

The orthogonal table L16(4⁵) was chosen for this test, and Table 4 shows the scheme, number and parameters chosen for the orthogonal test.

Table 3. Factor Level Table

Level	Factor	Applied pressure(A) (MPa)	Punch velocity(B) (mm/s)	Pouring temperature(C) (°C)	Mold preheating temperature(D) (°C)
1	50	30	660	150	
2	80	40	680	200	
3	100	50	700	250	
4	125	60	720	300	

Table 4. Test Scheme and Parameters

Number	Test number	Applied pressure(A) (MPa)	Punch velocity(B) (mm/s)	Pouring temperature(C) (°C)	Blank column	Mold preheating temperature(D) (°C)
1	16#	50	30	660	–	150
2	11#	50	40	680	–	200
3	6#	50	50	700	–	250
4	1#	50	60	720	–	300
5	9#	80	30	680	–	300
6	14#	80	40	660	–	250
7	3#	80	50	720	–	200
8	8#	80	60	700	–	150
9	7#	100	30	700	–	200
10	4#	100	40	720	–	150
11	13#	100	50	660	–	300
12	10#	100	60	680	–	250
13	2#	125	30	720	–	250
14	5#	125	40	700	–	300
15	12#	125	50	680	–	150
16	15#	125	60	660	–	200

Orthogonal Test Indicators

The hardness could reflect the comprehensive mechanical properties of the material. The as-cast squeeze casting hanger needs to be welded to the frame after CNC machining, so the as-cast hardness was more concerned. Therefore, the indicator in this test was the as-cast hardness of the hanger. The as-cast hardness could reflect the mechanical properties of the hanger.

Method of Analysis of Orthogonal Test Results

1. Range analysis

The advantage of the range analysis (RA) method was that it was more intuitive to determine the optimal level of the test and the primary and secondary relationship between the factors of the test on the index. In this paper, the three symbols K_i (i.e., the sum of the test results at any one level i), $K_{avg} i$ (the arithmetic mean of K_i , here $K_i/4$) and

R (extreme difference) were defined, where $R = \max\{K_{avg1}, K_{avg2}, K_{avg3}, K_{avg4}\} - \min\{K_{avg1}, K_{avg2}, K_{avg3}, K_{avg4}\}$.

2. Analysis of variance

Although RA was simple and intuitive, it cannot determine the significance of each factor on the test results because it cannot estimate the test error. Therefore, further significance analysis was required using analysis of variance (ANOVA). Multi-factor ANOVA was performed on the orthogonal test results using SPSS software, listing the ANOVA table, comparing the calculated F value with the critical value $F_{\alpha}(f_A, f_E)$, and then concluding whether it was significant or not, which could be divided into the following two cases.

1. If $F > F_{0.05}$, the effect of the factor was significant and was noted as “*”.
2. If $F \leq F_{0.05}$, the effect of the factor was not significant and was recorded as “(O)”.

Results and Analysis

Influence of Process Parameters on Microstructure and As-cast Hardness of the Motor Hangers

1. Effect of process parameters on as-cast hardness

Figure 3 shows the as-cast hardness of hanger parts numbered 1# to 16# obtained from the orthogonal test. The hardness of 8# is the highest at 73.2 HBW, while 9# and 16# have the lowest hardness at 67.2 HBW. The hardness value is closely related to machinability, indicating that hanger 8#, with the superior hardness, offers the best machinability. The technological parameters are as follows: applied pressure 80 MPa, punch velocity 60 mm/s, pouring temperature 700 °C and mold preheating temperature 150 °C. To delve deeper into the impact of squeeze casting process parameters on the as-cast hardness of the

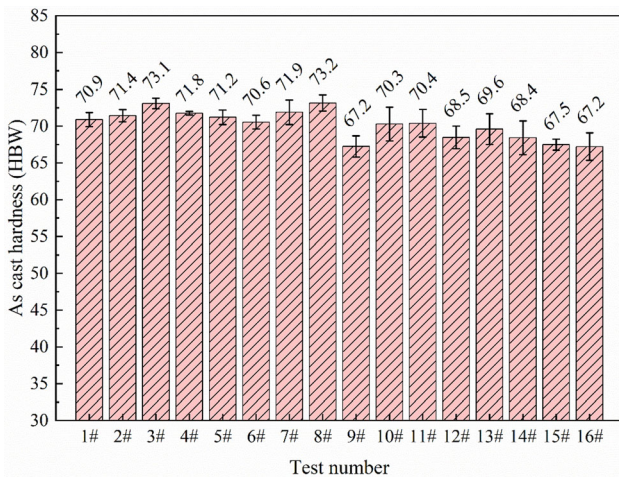


Figure 3. As-cast hardness under different experimental conditions.

hanger, both RA and ANOVA were conducted on the orthogonal test data.

(1) RA

Table 5 presents the results of the RA conducted in the orthogonal experiment to assess the as-cast hardness. From the table, it is evident that the factors affecting as-cast hardness are ranked in the following order of significance: pouring temperature > applied pressure > punch velocity > mold preheating temperature.

(2) ANOVA

Table 6 displays the ANOVA results of the orthogonal test for as-cast hardness. S_A^2 , S_B^2 , and S_D^2 are all smaller than S_E^2 , leading to factors A, B, and D are treated as errors, and the ANOVA table is recalculated accordingly.

The revised ANOVA results are shown in Table 7. The F distribution table shows that $F_{0.05}(3, 12) = 3.49$, $F_C(3, 12) = 9.475$, $F_C(3, 12) > F_{0.05}(3, 12)$. Therefore, factor C (pouring temperature) has a significantly effect the as-cast hardness value.

(3) Comprehensive analysis

The combination results from RA and ANOVA indicate that the pouring temperature has a significant effect on the as-cast hardness. In contrast, the applied pressure, punch velocity, and mold preheating temperature have insignificant effects. Figure 4 shows the average as-cast hardness of each factor at different levels. Based on Figure 4, it was inferred that the optimum technological parameters of squeeze casting for the applied pressure 100 MPa, punch velocity 40–60 mm/s, pouring temperature 700–720 °C, and mold preheating temperature 200 °C. Under the condition of ensuring mechanical properties, the faster the

Table 5. Range Analysis of As-cast Hardness Measurement Results by Orthogonal Test

Items	Levels	A	B	C	D
K-value	1	279.1	277.7	272.8	280.7
	2	282	281.9	276.4	282.9
	3	283.6	281.8	286.9	280.8
	4	278.6	281.9	287.2	278.9
K avg value	1	69.78	69.43	68.2	70.17
	2	70.5	70.47	69.1	70.72
	3	70.9	70.45	71.73	70.2
	4	69.65	70.48	71.8	69.73
Optimum levels		3	4	4	2
R		1.25	1.05	3.6	1
Number of levels		4	4	4	4
Number of replicates per level		4	4	4	4
Rank of factors		RC>RA>RB>RD			

Table 6. ANOVA of As-cast Hardness Measurement Results by Orthogonal Test

Differential source	Q	df	S ²	F	Significant
A	4.252	3	1.417	0.565	(O)
B	3.257	3	1.086	0.432	(O)
C	40.382	3	13.461	5.361	–
D	2.007	3	0.669	0.266	(O)
Errors	7.532	3	2.511		
Total	57.43	15			

Table 7. ANOVA of As-cast Hardness Measured by Recalculated Orthogonal Test

Differential source	Q	df	S ²	F	Significant
C	40.382	3	13.461	9.475	*
Errors	17.047	12	1.421		
Total	57.43	15			

filling speed, the easier it is to obtain a complete casting, so the best filling speed should be determined as 60 mm/s.

2. Influence of pouring temperature on as-cast microstructure

Based on the variance analysis, it is evident that the pouring temperature is the only significant factor influencing the mechanical properties of the sample, while the other factors are not significant. Table 6 that S_A^2 , S_B^2 , and S_D^2 were all smaller than S_E^2 , so it could be considered that the influences of A, B and D were the experimental error. Therefore, 16#, 11#, 6# and 1# samples were used to study the differences at different pouring temperatures. Figure 5 showcases scanning electron microscope images and energy spectrum surface scanning results of the as-cast microstructure observed at a pouring temperature of 720 °C. The analysis results for energy spectrum points at location 1 are detailed in Table 8. Based on the observations, the as-cast microstructure can be primarily segmented into three zones: A, B, and C. Zone A consists of coarse-grained α -Al. This began forming in the early solidification stage, driven by supercooling, leading to nucleation and growth, culminating in the creation of coarse dendrites. Zone B represents the eutectic structure formed during solidification. It predominantly comprises the Al–Si binary eutectic structure with a minor presence of the Al–Si–Mg ternary eutectic structure. The eutectic products are primarily the Al–Si eutectic phase¹⁹ and

Mg₂Si.²⁰ Zone C is characterized by a fine-grained structure made up of delicate Al grains with a smattering of eutectic silicon along its grain boundaries. This microstructure likely forms in the solidification's latter stages, with the feeding liquid being forcibly replenished into contraction vacancies due to pressure. Due to the late solidification time and high solute concentration of the feeding liquid, the molten metal solidifies under the dual effects of pressure supercooling and constitutional supercooling, forming a fine solidification structure. Since aluminum grains nucleate more and grow faster, Si atoms can't leave the liquid phase, and the growth of eutectic Si is hindered, which finally forms the morphology that eutectic Si is sparsely distributed on aluminum grain boundaries. From the results of the energy spectrum point analysis, it can be found that there are still a few phases containing Si, Mg, and Fe at the grain boundaries and eutectic clusters, which may be Mg₂Si,²¹ Al₅FeSi, and Al₈FeMg₃Si₆.²²

Through the above variance analysis, it is found that the only significant factor affecting the mechanical properties of the sample was pouring temperature, and the other factors are not significant. Of course, not being significant did not mean that it has no impact. However, it could be found from Table 6 that S_A^2 , S_B^2 , and S_D^2 are all smaller than S_E^2 , so it could be considered that the influences of A, B and D are the experimental error. Therefore, this paper selects 16#, 11#, 6# and 1# for comparative observation to study the influence of pouring temperature on microstructure and properties. Figure 6 displays the as-cast metallographic microstructure photographs of four samples selected from the orthogonal test group, each with different pouring temperatures. Specifically, they are 16# (660 °C, 67.2 HBW), 11# (680 °C, 70.4 HBW), 6# (700 °C, 70.6 HBW), and 1# (720 °C, 70.9 HBW). A comparison of these samples reveals that as the pouring temperature increases, the as-cast hardness also tends to rise. This trend aligns with the average values observed in the orthogonal test factors.

Figure 6a for the as-cast metallographic microstructure at 660 °C, the grains are mostly columnar dendritic crystals, there are clear secondary dendritic arms but undeveloped, and there are a large number of coarse eutectic clusters distributed between the grains. The low pouring temperature leads to rapid blocking of the pressure transfer channels, resulting in limited pressure acting on later solidification stages, and consequently, coarser grains are formed.

However, due to the low pouring temperature and short solidification time, it is too late to grow developed dendritic arms even with the lack of pressure subcooling, and

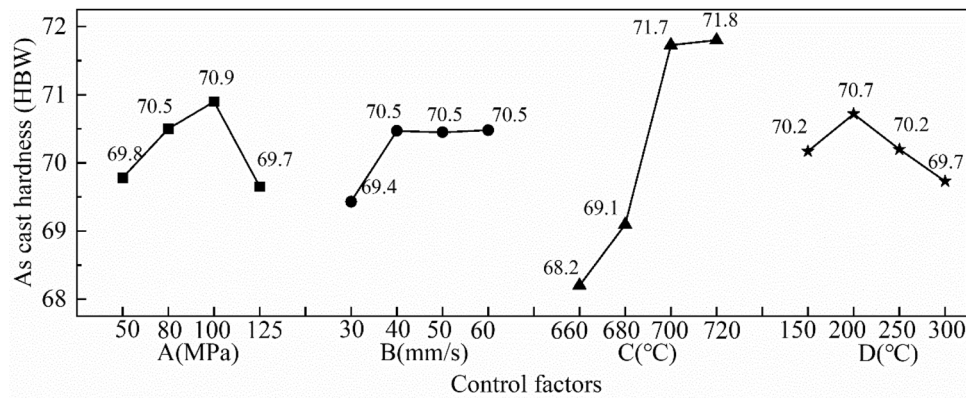


Figure 4. Mean value diagram of as-cast hardness at various levels.

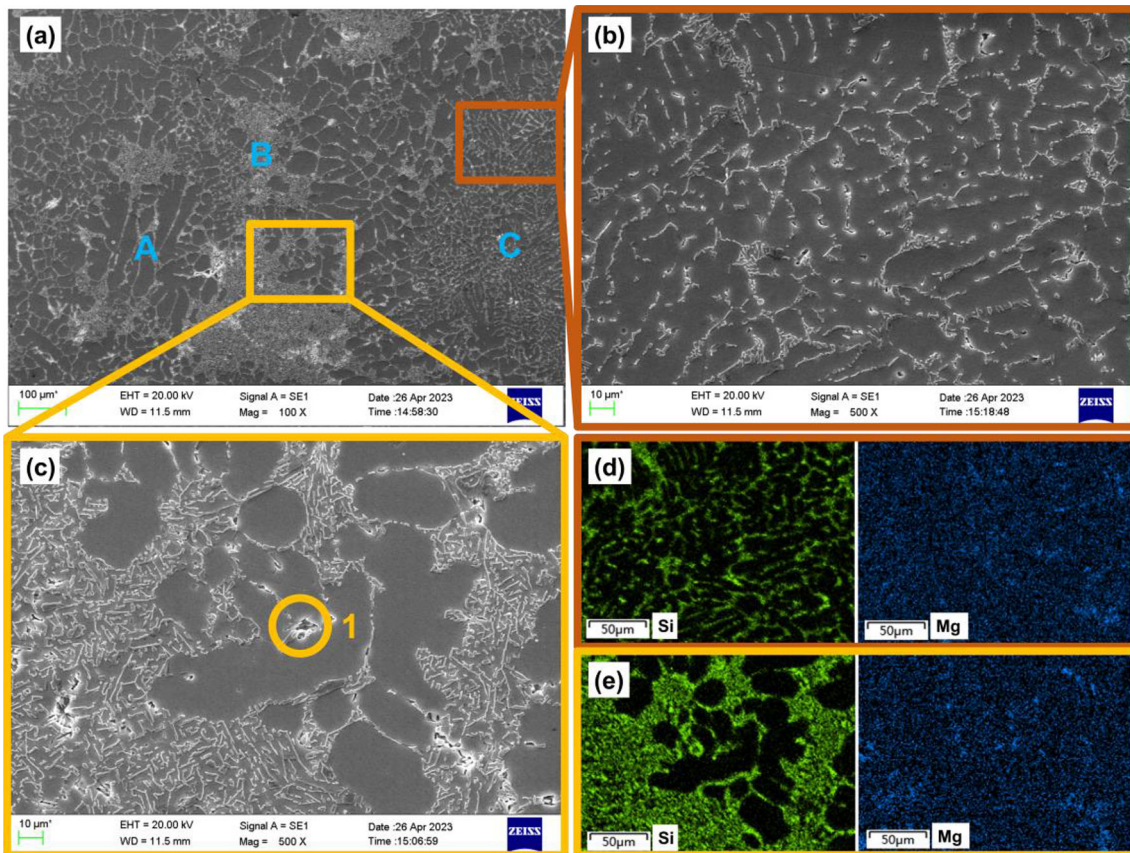


Figure 5. SEM photographs and mapping image of as-cast microstructure at pouring temperature of 720 °C: (a) 100 times morphology; (b) feeding microstructure; (c) eutectic microstructure and morphology; (d) EDS analysis image of the feeding tissue; (e) EDS analysis image of eutectic microstructure.

the final morphology of columnar dendritic crystals is presented. At 700 °C (Figure 6c), there's a noticeable reduction in grain size, with the appearance of a finer grain microstructure compared to those at 660 °C and 680 °C. This change can be attributed to the more effective opening of pressure transfer channels and the enhanced pressure effect due to the elevated temperature of the liquid

aluminum. Moreover, the eutectic cluster size at 680 °C is notably smaller than that in the 660 °C sample. This reduction is likely due to the pressure-induced decrease in the Si diffusion rate and the faster solidification of α -Al, which minimizes segregation. The phase diagram of hypoeutectic Al-Si alloys solidifying under high pressure shifts toward the Si phase side. This shift is influenced by

the pressure's effect on the diffusion coefficients of the elements in the melt. The equation for this is:

$$D = \frac{RT}{\delta\eta_0} \exp\left(-\frac{PV_0}{RT}\right) \quad \text{Eqn. 2}$$

where D is the diffusion rate; R is a constant; T is the temperature of the melt; δ is the free travel length of the atoms; η_0 is the viscosity of the melt at atmospheric pressure and the same temperature; P is the pressure; and V_0 is the original molar volume of the liquid phase.

It can be seen that the increase in pressure P leads to a decrease in the diffusion rate D of each element in the aluminum alloy, so that the solid solubility of Si in the Al matrix increases, inhibiting the solute buildup along the solid-liquid interface front, leading to a decrease in the tendency to form dendrites of α -Al, and so it is more likely to grow in the form of fine cytosol. In addition, by the thermodynamic basic relationship Eq.

$$\left[\frac{\partial(\Delta G_v)}{\partial P}\right]_T = V^L - V^S = \Delta V \quad \text{Eqn. 3}$$

where ΔG_v is the free energy; P is the pressure; V^L is the linear molar volume of liquid phase; and V^S is the linear molar volume of solid phase.

According to Eqn. 2, it can be seen that at a certain temperature, since $\Delta V > 0$ when Al solidifies and $\Delta V < 0$ when Si solidifies, Al is easier to nucleate and Si is more difficult to nucleate with the increase of pressure. Therefore, for the solidification process of Al-Si eutectic microstructure, the pressure will refine the Al grains and reduce the eutectic Si.

At 700 °C, as depicted in Figure 6c, there's a noticeable reduction in grain size, with the appearance of a finer grain microstructure compared to those at 660 °C and 680 °C. This change is attributed to the more effective opening of pressure transfer channels and the enhanced pressure effect due to the elevated temperature of the liquid aluminum. However, at 720 °C (Figure 6d), the solidification structure during filling becomes coarser compared to 700 °C, even though the fine grain structure appears finer. The slower solidification rate during filling results in coarser grains. Meanwhile, the higher solute concentration in the compensatory shrinkage solution leads to increased

Table 8. Results of Energy Spectrum Point Analysis for 1 Point

Elements	Mg	Al	Si	Fe
wt%	1.74	70.00	27.02	1.22

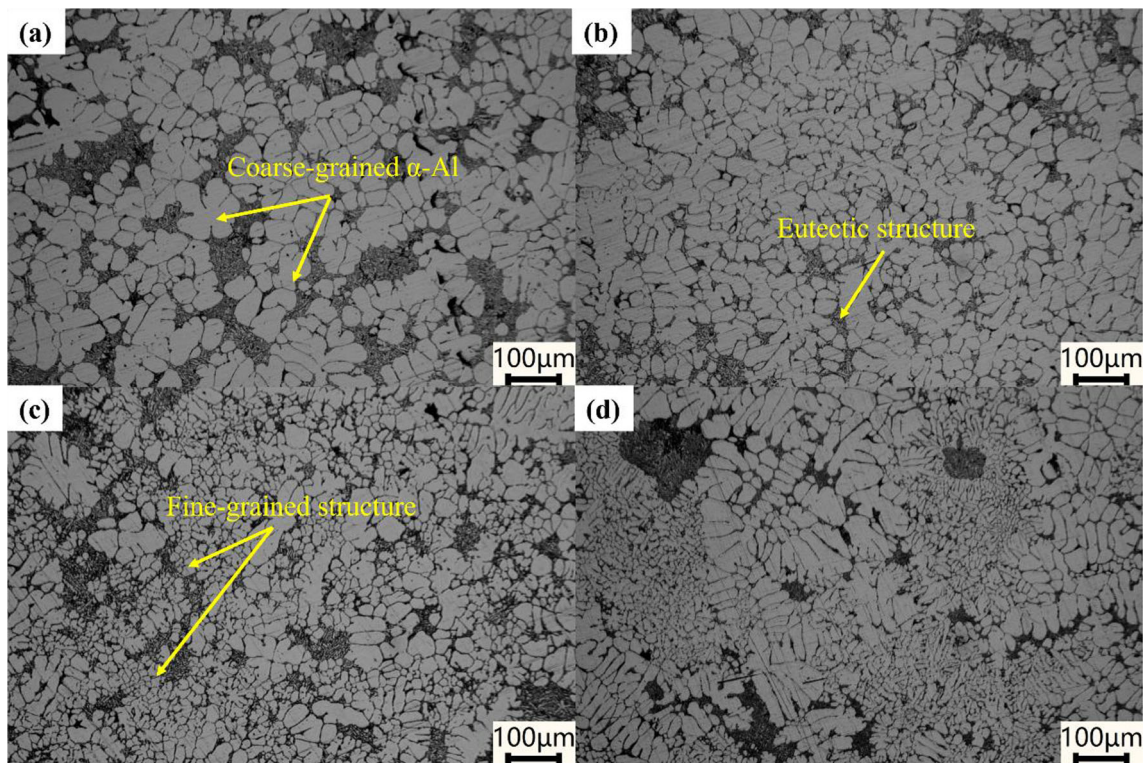


Figure 6. As-cast metallographic microstructure at different pouring temperatures in magnification of 200×: (a) 16#(660 °C); (b) 11#(680 °C); (c) 6#(700 °C); (d) 1#(720 °C).

compositional subcooling, resulting in a finer solidification structure during the compensatory shrinkage stage.

It can be found that the synergistic effect of pouring temperature and applied pressure has a significant impact on the microstructure of the casting, with the applied pressure affecting the microstructure and hence the performance of the hanger through the degree of openness of the pressure transfer channels. Notably, at 700 °C, the pressure transfer channels are fully open and the effect of pressure is most pronounced, resulting in the finest grains in the C zone (fine grain structure). This is an interesting finding on which this study further investigates the microstructure and properties of the hangers after heat treatment.

Effect of Pouring Temperature on Microstructure and Mechanical Properties of Hangers in T6 Heat Treatment Condition

The orthogonal test method pinpointed the pouring temperature as the primary factor influencing the as-cast hardness of the hangers. In contrast, the effects of punch velocity and mold preheating temperature on the as-cast hanger hardness were deemed insignificant. Similarly, the influence of process parameters on the properties of the hangers in the T6 heat treatment condition appears to be indirect, following the observed trends in the as-cast condition. Based on this understanding, it can be inferred that punch velocity, applied pressure, and mold preheating temperature also do not significantly affect the properties of the hangers in the T6 condition.

To investigate the impact of pouring temperature on the performance of hangers post T6 heat treatment, four sample groups (1#, 6#, 11#, and 16#) were selected for the T6 heat treatment. These samples were cast at respective pouring temperatures of 720 °C, 700 °C, 680 °C, and 660 °C, all under an applied pressure of 50 MPa. Since the orthogonal test analysis revealed that punch velocity and mold preheating temperature have minimal effects on the as-cast properties, strict control of these parameters was not required.

Effect of Pouring Temperature on the Hardness of T6 Heat Treatment Condition Hangers

Figure 7 shows the hardness of samples 16#(660 °C), 11#(680 °C), 6#(700 °C), 1#(720 °C) after T6 heat treatment. The bar charts show that the hardness initially increases with rising pouring temperature and then stabilizes. The 660°C group exhibits the lowest hardness at 94.2 HBW, while the 700°C group registers the highest at 99.1 HBW.

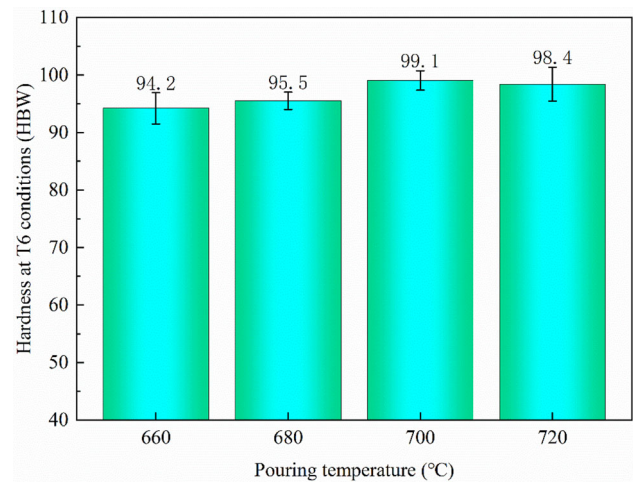


Figure 7. Hardness of T6 heat treatment at different pouring temperatures.

Effect of Pouring Temperature on the Tensile Strength of T6 Heat-Treated Condition Hangers

Figure 8 shows the tensile strength of samples 16#(660 °C), 11#(680 °C), 6#(700 °C), 1#(720 °C) after T6 heat treatment. It is evident from the graph that as the pouring temperature increases, the tensile strength first rises and then plateaus. The lowest strength is recorded in the 660 °C group, with a tensile strength value of 261 MPa, while the highest strength is observed in the 700 °C and 720 °C groups, both having a tensile strength value of 274 MPa. The tensile strength and hardness exhibit similar trends in response to varying pouring temperatures.

Effect of Pouring Temperature on the Percentage Elongation After Fracture of T6 Heat-Treated Condition Hangers

The percentage elongation after fracture of T6 hangers after heat treatment at different pouring temperatures is shown in Figure 9. As the pouring temperature rises, the percentage elongation after fracture initially remains stable, then increases, and subsequently decreases. The 700 °C group achieves the highest percentage elongation after fracture at 9.8%, while the 720 °C group records the lowest at 6.1%. To explain the changing trend caused by pouring temperature, the microstructure of the T6 hanger is observed.

Effect of Pouring Temperature on the Microstructure of Hanger T6 Heat Treatment Condition

Figure 10 presents the optical microscope images of the eutectic structure in the T6 state before and after heat

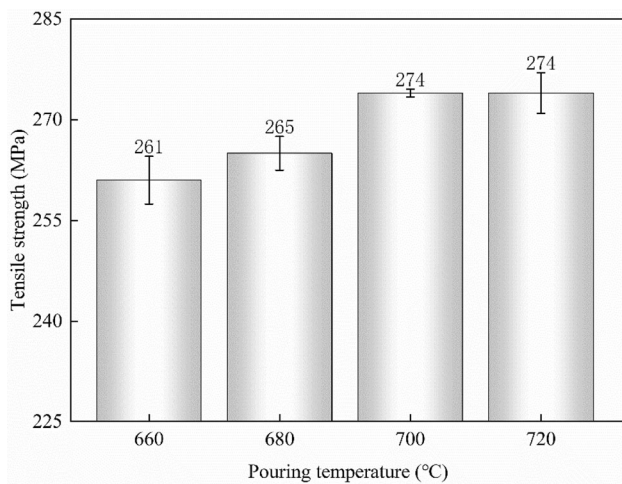


Figure 8. Tensile strength of samples prepared at different pouring temperatures after T6 heat treatment.

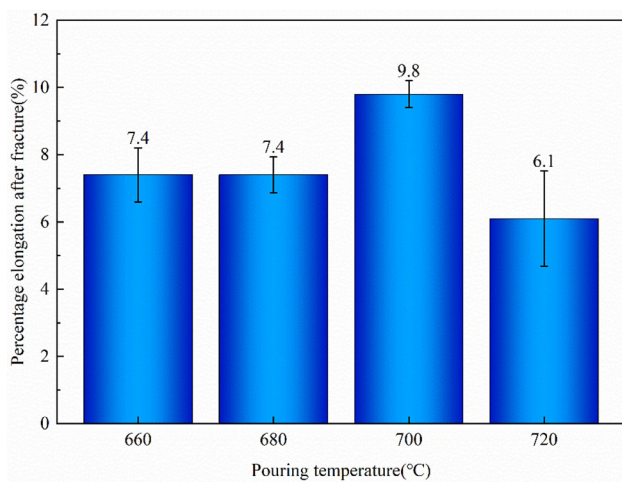


Figure 9. Percentage elongation after fracture at different pouring temperatures.

treatment at a pouring temperature of 720 °C. The eutectic Si exhibits a coarse needle-like and reticulated shape in the as-cast condition. During heat treatment, eutectic Si undergoes dissolution and granulation stages,^{23,24} leading to a transformation into spherical or coral-shaped structures. The eutectic Si after heat treatment is gradually spheroidized, mostly spherical or coral, so the properties of the squeeze casting parts are improved. Except that the morphology of eutectic silicon has changed to a certain extent, the other microstructures inherit the as-cast characteristics.

Photographs of the microstructure of the T6 state at a pouring temperature of 720 °C observed under the scanning electron microscope and the results of the energy

spectrum surface scanning are shown in Figure 11. Consistent with the as-cast microstructure, coarse crystalline α -Al (zone A), eutectic microstructure (zone B) and fine Al grains (zone C) are observed in the figure. From the map scanning results, it can be seen that the concentration of Si element is higher at point 2, which can be presumed to be primary crystalline Si.

Figure 12 shows the metallographic photographs of four groups of specimens, 16# (660 °C), 11# (680 °C), 6# (700 °C), and 1# (720 °C), after T6 heat treatment, and Figure 13 shows the SDAS values of their corresponding grains. By comparing Figures 12 and 6, it can be found that the morphology of the structures at different pouring temperatures after heat treatment still maintains the morphology of the as-cast state at the corresponding pouring temperatures, i.e., the pouring temperature does not directly affect the morphology of the T6 heat-treated structures but rather influences the as-cast structure and thus the T6 heat-treated structures further.

Furthermore, from Figure 13, it can be observed that the SDAS of the grains decreases initially and then basically stabilizes as the pouring temperature increases, which is consistent with the results of the previous intuitive analysis on the grain size of the as-cast microstructure. Notably, the change in grain size is the reason why its initial increase and subsequent stabilization of tensile strength and hardness after T6 heat treatment.

Figure 14 shows the photographs of the tensile fracture of T6 after heat treatment at different pouring temperatures observed under the scanning electron microscope.

As can be seen from the figure, a large number of tough dimples are visible in the fracture of the specimens at the four pouring temperatures, so it can be judged that the fracture forms at the four temperatures are all toughness fractures. However, some cleavage steps are also found in the four figures, which may be the fracture traces of some of the brittle phases (e.g., eutectic silicon and Fe-containing phases). Figure 14c has the smallest tough dimples and fewer cleavage steps, which explains the highest elongation after fracture in the 700 °C group. In Figure 14d, although there are a large number of fine tough nests, there are also many brittle phases which, in combination with Figures 5 and 11, are directly responsible for the lowest plasticity in the 720 °C group.

Based on the above microstructure and mechanical properties, compared with the pouring temperature of 720 °C, the pouring temperature of 700 °C was better.

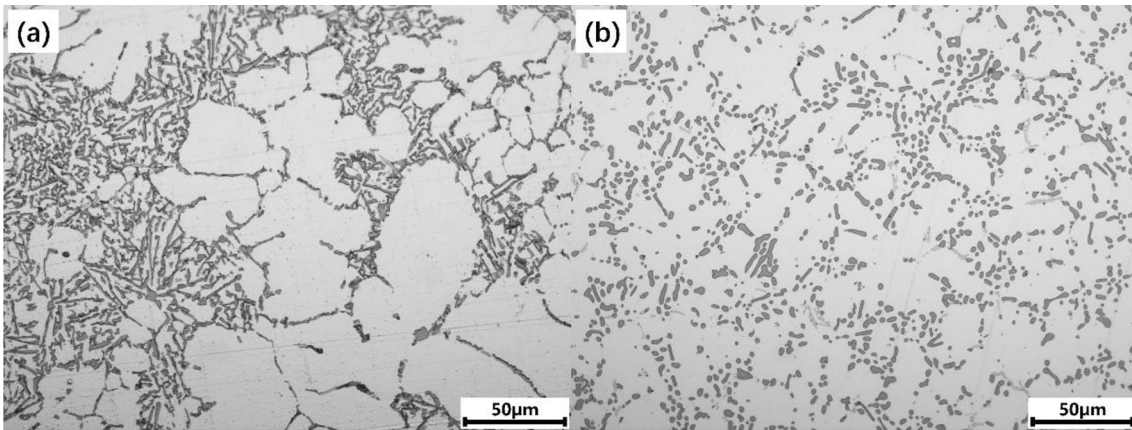


Figure 10. Eutectic microstructure before and after heat treatment at pouring temperature of 720 °C in magnification of 500×: (a) Microstructure before heat treatment; (b) Microstructure after heat treatment.

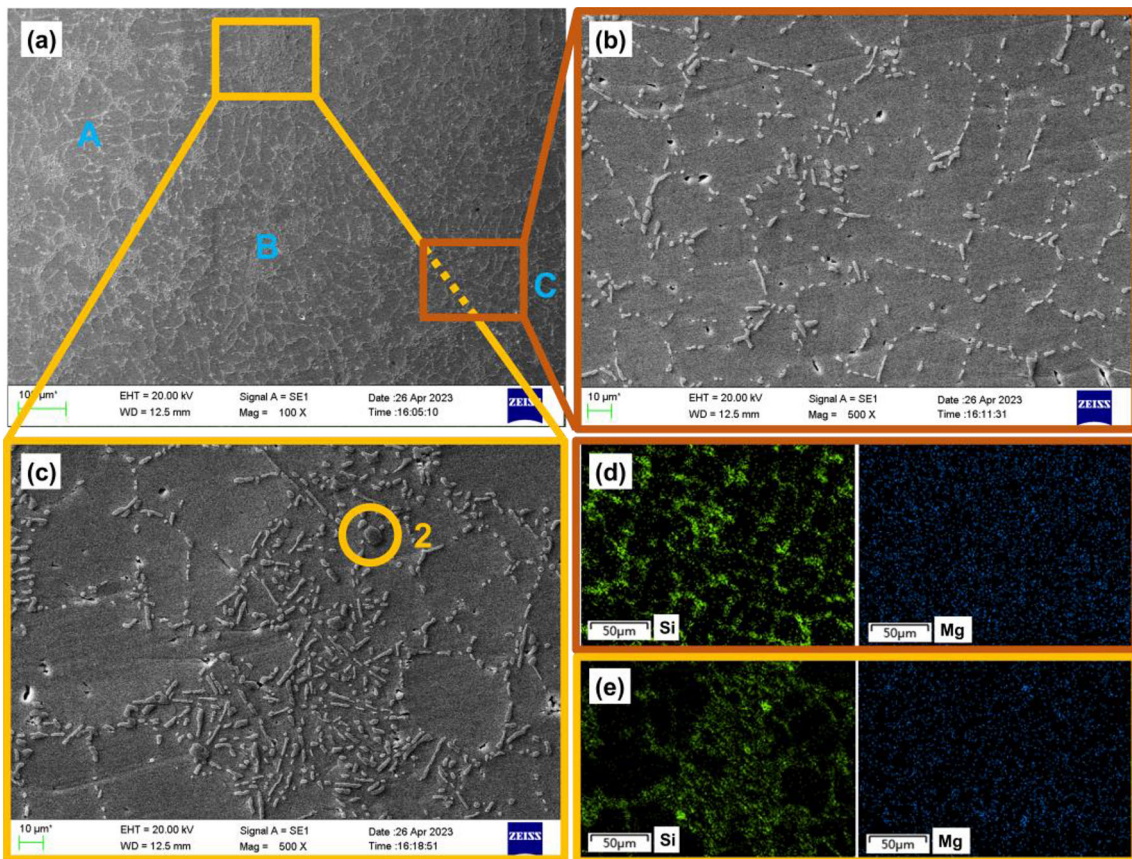


Figure 11. SEM photographs and mapping image of microstructure after T6 heat treatment at pouring temperature of 720 °C: (a) 100 times morphology; (b) feeding microstructure; (c) eutectic microstructure and morphology; (d) EDS analysis image of the feeding tissue; (e) EDS analysis image of eutectic microstructure.

Properties Test of Squeeze Casting Hanger Under Optimum Process Parameters

Figure 15a presents the squeeze casting hanger produced based on the optimal process parameters determined in the previous analysis, which included an applied pressure of

100 MPa, a punch velocity of 60 mm/s, a pouring temperature of 700 °C, and a mold preheating temperature of 200 °C. Figure 15b is a hanger produced by forging process. The mechanical properties of the squeeze casting hanger after T6 heat treatment were tested and compared with those of the forged hanger, as shown in Figure 16.

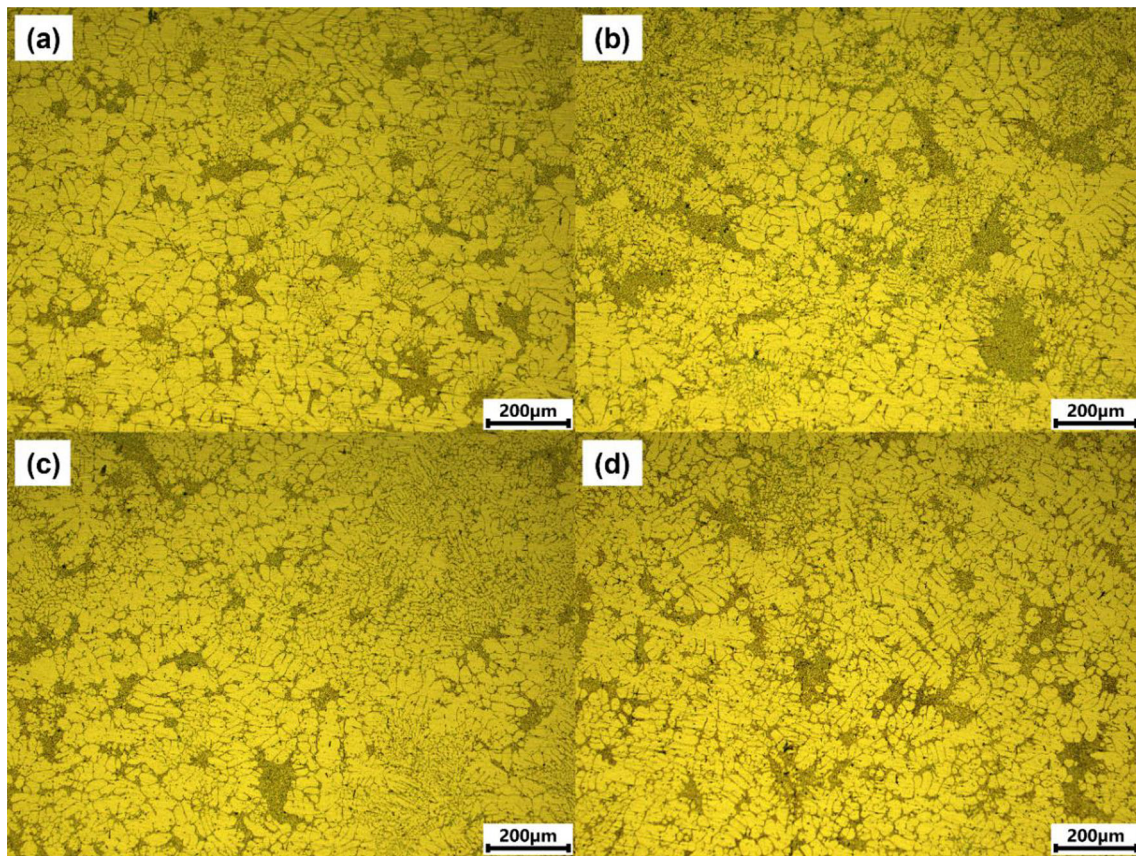


Figure 12. Metallographic microstructure of T6 heat treatment at different pouring temperatures in magnification of 100×: (a) 16#(660 °C); (b) 11#(680 °C); (c) 6#(700 °C); (d) 1#(720 °C).

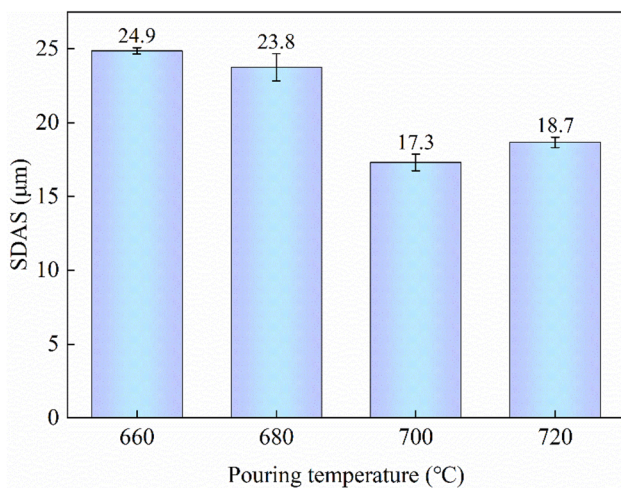


Figure 13. SDAS of microstructure after T6 heat treatment at different pouring temperatures.

The tensile strength of the hanger produced by squeeze casting was 297 MPa, the percentage elongation after fracture was 10.2%, the hardness was 105 HBW. The mechanical properties were close to those of the hanger produced by forging. The tensile strength, percentage elongation after fracture, and Brinell hardness of the hanger produced by forging are 304 MPa, 17%, and 103 HBW, respectively, as shown in Figure 16.

Conclusions

In this study, the influence of indirect squeeze casting parameters on the microstructure and mechanical properties of motor hangers is investigated and the following conclusions are obtained:

- (1) Orthogonal testing underscores the pouring temperature as a pivotal determinant of as-cast hardness, whereas applied pressure, punch velocity, and mold preheating temperature exert insignificant influence. Of the 16 orthogonal sets, set 8# manifests the apex as-cast hardness at 73.2 HBW, characterized by 80 MPa pressure, 60 mm/s punch velocity, 700 °C pouring temperature, and 150 °C mold preheat. In conjunction with RA, the conjectured optimal parameters for peak as-cast hardness encompass 100 MPa pressure, 60 mm/s punch speed, 700 °C pouring temperature, and 200 °C mold preheat.
- (2) The study examines the influence of pouring temperature on the microstructure and properties of the hanger in both cast and T6 states. It was observed that the hardness of the hanger in the T6 state initially rose with increasing pouring

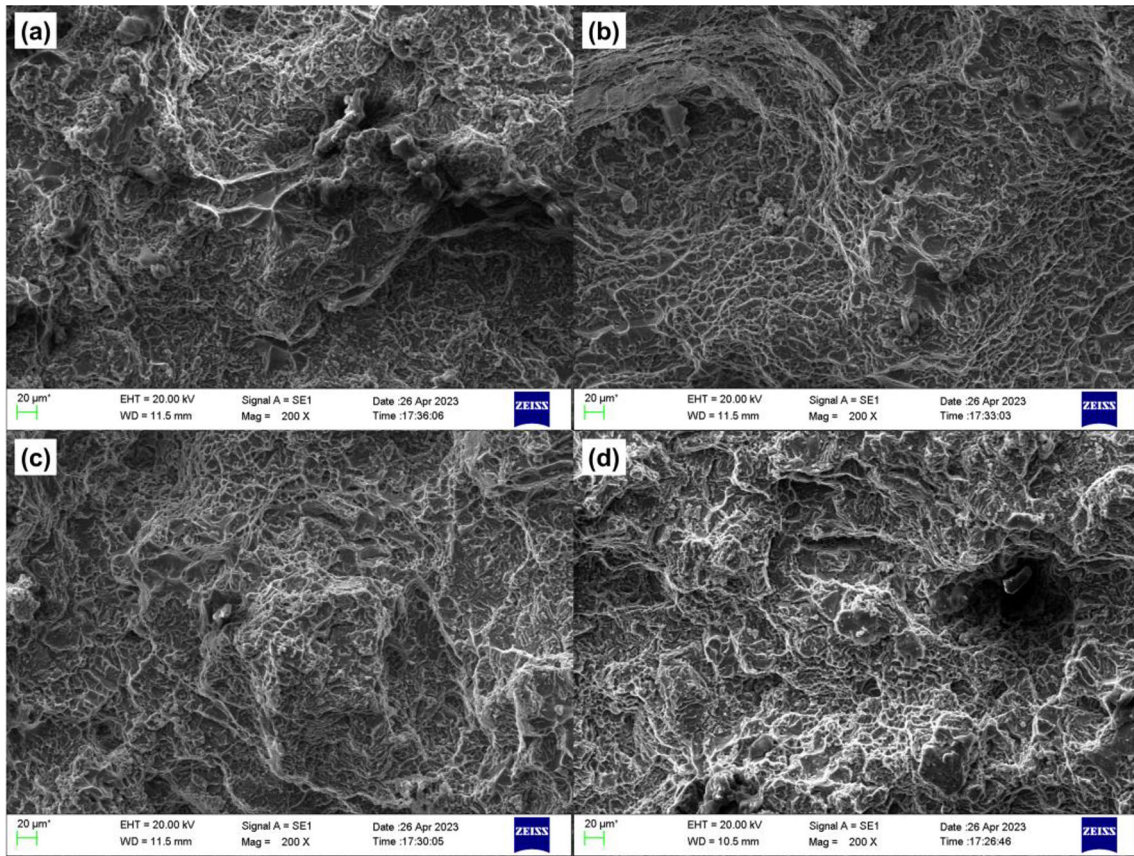


Figure 14. SEM photographs of tensile fracture of samples prepared at different pouring temperatures after T6 heat treatment: (a) 16#(660 °C); (b) 11#(680 °C); (c) 6#(700 °C); (d) 1#(720 °C).

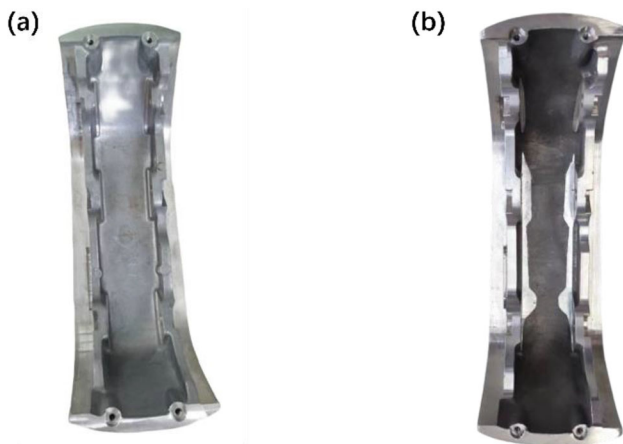


Figure 15. Photograph of motor hanger product. (a) Made by squeeze casting process; (b) made by forging process.

temperature, then plateaued. This trend mirrored the effects on as-cast hardness and T6 tensile strength. The microstructure in both states can be categorized into three domains: coarse-grained α -Al (A region), eutectic structure (B region), and fine-grained structure (C region). Elevated pouring temperatures enhance pressure

transmission channels, facilitating the flow of shrinkage liquid into vacancies, refining the grain structure in the C region and bolstering mechanical properties. However, excessive pouring temperatures enlarge α -Al grains in the A region, detrimentally impacting the properties.

- (3) It is found that the process parameters do not have a direct effect on the properties of the squeeze-cast hangers after heat treatment, and the as-cast features are retained after T6 heat treatment except that the morphology of eutectic silicon becomes short and rounded. Therefore, the process parameters are indirectly affecting the properties after heat treatment by affecting the as-cast structure. Consequently, for heat-treatable reinforced aluminum alloys, the as-cast microstructure serves as a direct metric to evaluate the efficacy of the squeeze casting process.
- (4) Under the optimal process parameters, the tensile strength of the hanger is 297 MPa, the percentage elongation after fracture is 10.2%, the hardness is 105 HBW.

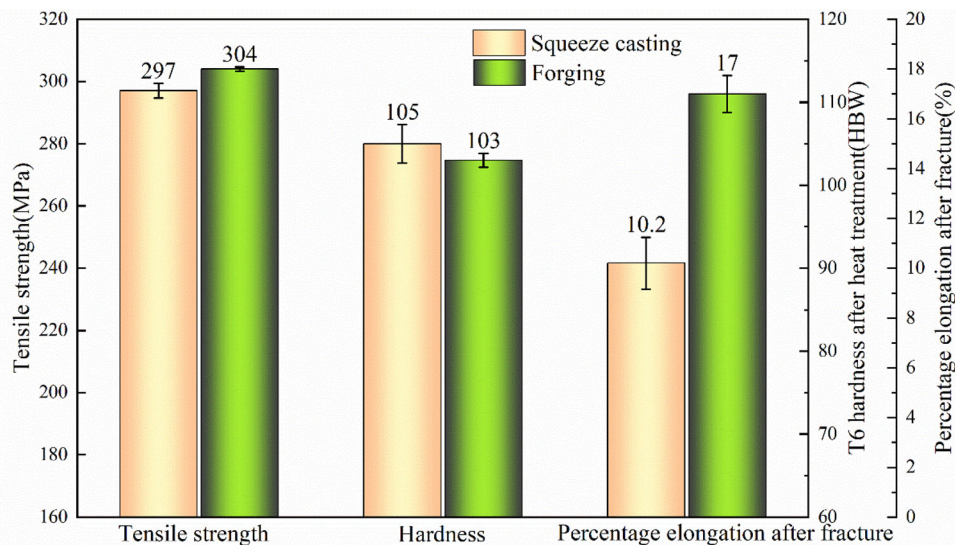


Figure 16. Mechanical properties of squeeze casting hanger and forging hanger.

Author Contributions XJ: Writing—original draft, Conceptualization, Investigation, Data curation. SX: Writing—review & editing, Conceptualization. HS: Methodology, Validation and Writing. GY: Investigation. QH: Validation.

Funding

No funding was received to assist with the preparation of this manuscript.

REFERENCES

1. Y.Y. Li, W.W. Zhang, H.D. Zhao et al., Research progress on squeeze casting in China. *China Foundry* **11**(4), 239–246 (2014).
2. M.R. Ghomashchi, A. Vikhrov, Squeeze casting: an overview. *J. Mater. Process. Technol.* **101**(1), 1–9 (2000). [https://doi.org/10.1016/S0924-0136\(99\)00291-5](https://doi.org/10.1016/S0924-0136(99)00291-5)
3. S.W. Youn, C.G. Kang, P.K. Seo, thermal fluid/solidification analysis of automobile part by horizontal squeeze casting process and experimental evaluation. *J. Mater. Process. Technol.* **146**(3), 294–302 (2004). <https://doi.org/10.1016/j.jmatprotec.2003.11.005>
4. H.B. Yang, X.S. Zhao, W.Z. Fan et al., Development status and applications prospect of squeeze casting technology. *Adv. Mater. Res.* **538–541**, 1154–1157 (2012). <https://doi.org/10.4028/www.scientific.net/AMR.538-541.1154>
5. O.O. Edosa, F.K. Tekweme, K. Gupta, Squeeze casting for metal alloys and composites: an overview of influence of process parameters on mechanical properties and microstructure. *China Foundry* **20**, 148–158 (2023). <https://doi.org/10.1007/s41230-022-2030-1>
6. M. Kiuchi, Recent trend of squeeze casting. *Tetsu-to-Hagané* **71**(1), 12–18 (1985). https://doi.org/10.2355/tetsutohagane1955.71.1_12. (in Japanese)
7. R.X. Li, L.J. Liu, L.J. Zhang, J.H. Sun, Y.J. Shi, B.Y. Yu, Effect of squeeze casting on microstructure and mechanical properties of hypereutectic Al–xSi alloys. *J. Mater. Sci. Technol.* **33**(4), 404–410 (2017). <https://doi.org/10.1016/j.jmst.2017.02.004>
8. A. Karthik, R. Karunanithi, S.A. Srinivasan, M. Prashanth, The optimization of squeeze casting process parameter for AA2219 alloy by using the Taguchi method. *Mater. Today Proc.* **27, Part 3**, 2556–2561 (2020). <https://doi.org/10.1016/j.matpr.2019.10.136>
9. P. Senthil, K.S. Amirthagadeswaran, Optimization of squeeze casting parameters for non symmetrical AC2A aluminium alloy castings through Taguchi method. *J. Mech. Sci. Technol.* **26**, 1141–1147 (2012). <https://doi.org/10.1007/s12206-012-0215-z>
10. Q.M. Chang, C.J. Chen, S.C. Zhang, D. Schwam, J.F. Wallace, Effects of process parameters on quality of squeeze casting A356 alloy. *Int. J. Cast Met. Res.* **23**(1), 30–36 (2010). <https://doi.org/10.1179/174313309X449309>
11. S.B. Bin, S.M. Xing, L.M. Tian et al., Influence of technical parameters on strength and ductility of AlSi₉Cu₃ alloys in squeeze casting. *Trans. Nonferrous Met. Soc. China (Engl. Ed.)* **23**(4), 977–982 (2013). [https://doi.org/10.1016/S1003-6326\(13\)62555-8](https://doi.org/10.1016/S1003-6326(13)62555-8)
12. C.F. Zhao, H.Y. Xu, Z.S. Ji, Hu.M.L. Wei Liu, B. Jiang, Effect of near-liquidus squeeze casting temperature on microstructure and mechanical property of AZ91D alloy differential support. *Mater. Lett.* **270**, 127681 (2020). <https://doi.org/10.1016/j.matlet.2020.127681>
13. A. Maleki, B. Niroumand, A. Shafyei, Effects of squeeze casting parameters on density, macrostructure and hardness of LM13 alloy. *Mater. Sci. Eng. A* **428**(1–2), 135–140 (2006). <https://doi.org/10.1016/j.msea.2006.04.099>

14. V. Dao, S. Zhao, W. Lin, C. Zhang, Effect of process parameters on microstructure and mechanical properties in AlSi₉Mg connecting-rod fabricated by semi-solid squeeze casting. *Mater. Sci. Eng. A* **558**, 95–102 (2012). <https://doi.org/10.1016/j.msea.2012.07.084>
15. A. Maleki, A. Shafyei, B. Niroumand, Effects of squeeze casting parameters on the microstructure of LM13 alloy. *J. Mater. Process. Technol.* **209**(8), 3790–3797 (2009). <https://doi.org/10.1016/j.jmatprotec.2008.08.035>
16. E. Hajjari, M. Divandari, An investigation on the microstructure and tensile properties of direct squeeze cast and gravity die cast 2024 wrought Al alloy. *Mater. Des.* **29**(9), 1685–1689 (2008). <https://doi.org/10.1016/j.matdes.2008.04.012>
17. A.R. Ravikumar, K.S. Amirthageswaran, P. Senthil, Parametric optimization of squeeze cast AC2A-Ni coated SiC_p composite using Taguchi technique. *Adv. Mater. Sci. Eng.* **2014**, 1–10 (2014). <https://doi.org/10.1155/2014/160519>
18. J.X. Deng, B. Xie, D.D. You et al., Process parameters design of squeeze casting through an improved KNN algorithm and existing data. *J. Manuf. Process.* **84**, 1320–1330 (2022). <https://doi.org/10.1016/j.jmapro.2022.10.074>
19. L. Snugovsky, J.F. Major, Silicon segregation in aluminium casting alloy. *Mater. Sci. Technol.* **16**(2), 125–128 (2000). <https://doi.org/10.1179/026708300101507604>
20. B. Dang, C.C. Liu, F. Liu et al., Effect of as-solidified microstructure on subsequent solution-treatment process for A356 Al alloy. *Trans. Nonferrous Met. Soc. China* **26**(3), 634–642 (2016). [https://doi.org/10.1016/S1003-6326\(16\)64152-3](https://doi.org/10.1016/S1003-6326(16)64152-3)
21. J.J. Kim, D.H. Kim, K.S. Shin et al., Modification of Mg₂Si morphology in squeeze cast Mg–Al–Zn–Si alloys by Ca or P addition. *Scr. Mater.* **41**(3), 333–340 (1999). [https://doi.org/10.1016/s1359-6462\(99\)00172-4](https://doi.org/10.1016/s1359-6462(99)00172-4)
22. P. Suwanpinij, U. Kitkamthorn, I. Diewwanit et al., Influence of copper and iron on solidification characteristics of 356 and 380-type aluminum alloys. *Mater. Trans.* **44**(5), 845–852 (2003). <https://doi.org/10.2320/matertrans.44.845>
23. F. Paray, J.E. Gruzleski, Modification—a parameter to consider in the heat treatment of Al–Si alloys. *Cast Met.* **5**(4), 187–198 (1992). <https://doi.org/10.1080/09534962.1992.11819112>
24. H.J. Sun, S.M. Xing, B.W. Zhao et al., Study on the influence of solution temperature on the synergistic effect of precipitation strengthening and fine grain strengthening of AA6061. *Mater. Today Commun.* **33**, 104312 (2022). <https://doi.org/10.1016/j.mtcomm.2022.104312>

Publisher's Note Springer Nature remains neutral with regard to jurisdictional claims in published maps and institutional affiliations.

Springer Nature or its licensor (e.g. a society or other partner) holds exclusive rights to this article under a publishing agreement with the author(s) or other rightsholder(s); author self-archiving of the accepted manuscript version of this article is solely governed by the terms of such publishing agreement and applicable law.